Forest Plot Decay Level Classification from ALS-Derived L-moments

Abubakar Sani-Mohammed[a], Wei Yao[a,b], Reda Fekry[c], Tsz-Chung Wong[a], Marco Heurich[d,e,f]

[a] Department of Land Surveying and Geo-Informatics, The Hong Kong Polytechnic University, Hung Hom, Kowloon, Hong Kong.

[b] The Hong Kong Polytechnic University Shenzhen Research Institute, Shenzhen, China.

[c] Department of Geomatics Engineering, Faculty of Engineering at Shoubra, Benha University, Egypt.

[d] Department for National Park Monitoring and Animal Management, Bavarian Forest National Park, 94481 Grafenau, Germany.

[e] Chair of Wildlife Ecology and Management, Faculty of Environment and Natural Resources, University of Freiburg, Freiburg, Germany.

[f] Department of Forestry and Wildlife Management, Campus Evenstad, Inland Norway University of Applied Sciences, Koppang, Norway.

Keywords: LiDAR metrics, ALS, L-moments, Plot decay levels, Forest management, Forest sustainability, Biodiversity, Deadwood.

Abstract

Forests play key roles in climate regulation and essential environmental services for living organisms. This is why forests are the central focus of the United Nations (UN) Sustainable Development Goal (SDG 15). Thus, effective forest management is critical for forest sustainability and preservation. Remote sensing advancements have improved forest mensuration leveraging cost and time, contrary to the field surveying approach. Often, field data is required to validate remotely sensed results. However, circumstances in the forest may render field data collection impossible. This study applied LiDAR-derived L-moments to directly estimate and classify five forest plot decay levels, to understand forest growth dynamics in the absence of field data. Two L-moment-based rules were tested and evaluated for classifying the plot decay levels from ALS height returns. Our findings show that the first rule ($Lcv = 0.5$) classified decay Levels 1 and 2 at $Lcv < 0.5$ and Levels 3 to 5 at $Lcv > 0.5$, while the second rule ($Lskew = 0$) classified decay Level 1 at $Lskew < 0$, and Levels 2 to 5 at $Lskew > 0$. This indicates that, while discriminating plot decay levels, the L-moment-based rules can classify healthy forest areas and areas of deadwood of varying decay levels directly from ALS height returns. This can be convenient for forest managers to exploit for classifying plot decay levels and for mapping areas of large gaps for planning forest resources for effective forest management. Furthermore, the approach can equally be significant for assessing forest biomass, biodiversity, and carbon stock.

1. Introduction

Forests cover about 31% of the world’s total land area, out of which 93% are natural forests and the rest are planted (FAO, 2020). Forests play a key role in regulating a clean climate and thus serve as the backbone of natural ecosystems (Millar and Stephenson, 2015, Gauthier et al., 2015, Wingfield et al., 2015, Hansen et al., 2013). Thus, understanding forest growth dynamics is very important for effective forest management, which is critical to forest sustainability and preservation.

Forests experience disturbances due to biotic, abiotic, and anthropogenic activities (Millar and Stephenson, 2015, Curtis et al., 2018, Gauthier et al., 2015, Sugden et al., 2015). This can cause serious effects resulting in tree mortality like tree infections and decay, leading to a reduction in productivity, and eco- system services (Keen, 1955, Thomas, 1979, Millar and Stephenson, 2015). Forest tree decay begins when trees die. Subsequently, defoliation, twigs, and branch breakages as well as broken tops are frequently seen in varying degrees based on the level of decay, to the extent that trees become snags (Thomas, 1979). Thus, monitoring and mapping forest tree decay levels is vital for understanding forest growth dynamics and for effective forest resource management. Furthermore, this can equally be significant for biodiversity, biomass, and carbon stock assessments.

Monitoring natural forests is more challenging than plantations because plantations are often single species (Wingfield et al., 2015) while natural forests consist of numerous species. Another reason is the variations in landscape, tree spatial distribution and density, and biodiversity. Advancement in remote sensing has improved forest observations from long-range measurements, leveraging time and cost (White et al., 2016), contrary to the classical field surveying approach. Consequently, forest managers and practitioners frequently use remote sensing data and techniques for forest health mensuration and monitoring (Curtis et al., 2018, Lausch et al., 2017, Lausch et al., 2016, Sani-Mohammed et al., 2022). However, it has been a normal practice to have field data for supporting remotely sensed data in analyzing and validating results. Nonetheless, it is also argued that circumstances such as floods, unfavorable topography, wild animals, and some natural phenomena could delay and/or make field surveying impossible in several parts of the forest. Therefore, the need for

a tested convenient optional approach to understanding forest growth dynamics without using field data cannot be underestimated, albeit coupled with expert advice.

The introduction of the Light detection and ranging (LiDAR) sensor (Dong and Chen, 2017, Drake et al., 2002, Lefsky et al., 2002b) has enabled forest mensuration in 3D with higher resolution and accuracy (contrary to the optical sensors) in the form of point clouds. LiDAR measurements are from pulse signal returns in full waveform (Yao et al., 2012) or discrete returns (Teobaldelli et al., 2017). Airborne Laser Scanning (ALS) is a LiDAR-based system mounted on aircraft for forest mensuration from above. Contrary to Terrestrial Laser Scanning (TLS), ALS has the advantage of measuring above-ground biomass with a larger coverage area (Dubayah and Drake, 2000, Lefsky et al., 2002a). This makes ALS more convenient for measuring larger forest areas.

Research has established that ALS-derived L-moments can directly classify forest structural features, which can be significantly convenient to forest managers in the absence of field data (Valbuena et al., 2017). Forest tree decay biophysically changes trees’ structural features and forest stands dynamics. Cognizant of this fact, it is hypothesized that, based on L-moments (Hosking, 1989), ALS height returns can conveniently estimate and classify forest plot decay levels using L-moment-based rules (Valbuena et al., 2017) in the absence of field data. Therefore, this study evaluated the L-moment-based rules for classifying five plot decay levels in the Bavarian Forest National Park (BFNP) (Figure 1). While this approach can be a convenient option for forest managers to assess and plan forest resources and biodiversity, it can equally be a cost-effective way of understanding forest growth dynamics for effective forest management and preservation.

2. Materials and Methods

2.1 Study area

The BFNP (Figure 1) natural mixed forest in Southeastern Germany was the study area. The forest has an area of about 242.5 km2 and shares boundaries with the Czech Republic at 49.10 degrees North, and 13.22 degrees East. The park was established in the 1970s aiming to prevent anthropogenic activities in the forest to protect its natural processes (Nielsen et al., 2014, Sani-Mohammed et al., 2022). The forest has undulating terrain with heights varying between about 600 and 1455 m. This makes field surveying challenging. Most of the plant species are conifers, dominated by the Norway Spruce *(Picea abies)*; other species include the European silver fir *(Abies alba)*, and European Beech *(Fagus sylvatica)* (van der Knaap et al., 2020).

2.2 Data acquisition

Three transects (Figure 1) of ALS data were acquired using a Riegle LMS-Q680i-400 kHz scanner during a flight on 18th August 2016, at about 300 m high above sea level. The raw data was preprocessed and transformed to fit the Gauss-Kruger coordinate system (EPSG = 31468; DHDN 3-Degree Gauss zone 4) in LAZ 1.2 format. The resulting point cloud had a greater than 70 points per square meter sampling rate.

CIR imagery (20 cm ground resolution) with three spectral bands (NIR, R, G) was used to augment the ALS data for spectral visualization in examining the five plot decay levels. The imagery was acquired using a Cessna 207 aircraft with DMC 122 camera at an average height of 2918 m above mean sea level. Radiometric correction and orthorectification were applied to the imagery Trimble’s OrthoBox (orthovista Orthomaster).

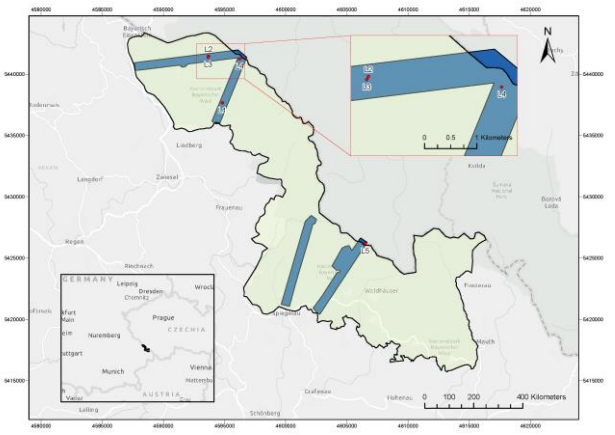

Figure 1. The BFNP map (green) illustrating the ALS transacts (blue) and the selected plots (red).

2.3 Data processing and plot selection

The ALS point clouds were fused with the CIR imagery for visual inspection of tree canopies and examining plots of varying decay levels. This combination was considered to exploit the spectral values of the CIR imagery to differentiate, especially, between the healthy trees and deadwood. Since ALS does not have the color effect, differentiating between decay levels is challenging, especially for Levels 1 (healthy trees) and 2 (early-stage dead trees). Then, five decay levels (Level 1 to Level 5; Figure 2) were examined from mature stands and selected, taking inspiration from Thomas’ description (Thomas, 1979, Sani-Mohammed et al., 2023, Wong et al., 2023) and based on visual interpretation of combined ALS point clouds and CIR imagery, at a 30 m radius plot level. Detailed descriptions of the plot decay levels are presented in Table 1, while Figure 2 displays the five decay levels resulting from combined ALS and corresponding CIR imagery. Table 2 presents the vertical distributions of the geometric ALS metrics (Roussel et al., 2020) of point clouds for each of the 30 m plots. Subsequently, we created five more subplots from each of the main plots. These subplots were created from the centre with radii of 5, 10, 15, 20, and 25 m making 30 plots in total (6 plots for each decay level). After examining, identifying, and selecting plot decay levels, the remainder of the processing was conducted using only ALS point clouds. The Cloth Simulation Function (CSF) algorithm (Zhang et al., 2016) was used to classify ground points before generating Digital terrain models (DTMs). The point clouds were normalized to the ground points and DTMs before deriving the ALS-based L-moments.

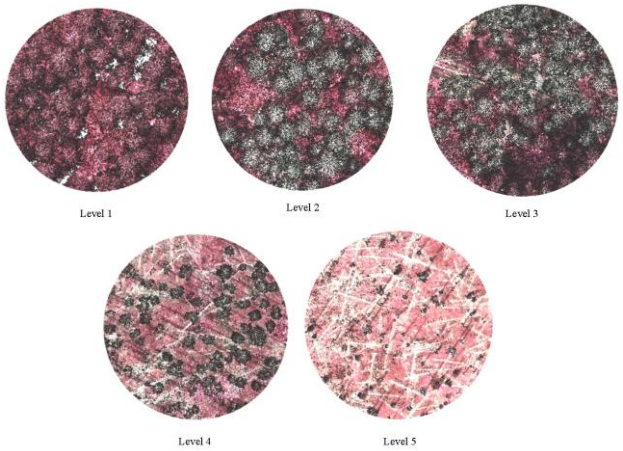

Figure 2. The five plot (30 m radius) decay levels displayed from combined ALS point clouds and CIR imagery. The reddish-to-brown crowns indicate healthy trees while gray/dark gray to green indicate dead trees.

Decay Level	Description
Lv 1	All healthy trees without remnants of de- cay. Tree crowns are spectrally seen in red- dish to brown color from the CIR imagery. Plots have closed canopied due to thick and heavy foliage and branches.
Lv 2	Dead trees at early stages with small or no defoliation. Tree crowns are detected due to a color change from gray to green.
Lv 3	Dead trees with more defoliation. Tree crowns are detected due to biophysical changes in color (gray to green) and size (reduction due to fallen leaves, broken branches, and in some cases treetops).
Lv 4	Dead trees with heavy defoliation with several broken twigs and branches. Tree crowns are detected due to biophysical changes in color and size. Fallen logs and many broken treetops are seen. Trees are fast approaching snag level as larger gaps are seen between deadwoods.
Lv 5	Snag dominated and deadwood. Almost all branches and twigs cleared. Many dead- woods are broken to the stem level. Fallen log traces are seen lying on the ground.

Table 1. Description of the plot decay levels.

Decay Level	No. of points	Ground points (%)	H_{mean} (m)	H_{max} (m)	SD
Lv 1	285919	11.8	21.3	41.9	10.6
Lv 2	405106	12.8	12.2	36.4	9.26
Lv 3	597143	21.6	10.9	34.2	9.1
Lv 4	390399	66.5	3.66	28.9	6.15
Lv 5	157362	88.5	0.67	20.9	2.71

Table 2. The vertical distribution of the geometric ALS metrics of point clouds for each of the 30 m radius plots. H_{mean} = Mean height; H_{max} = Maximum height; SD = Standard deviation

2.4 The L-moment-based rules

L-moments are metrics that are statistically derived from linear combinations of order statistics (Hosking, 1990, Hosking, 1989). They are less susceptible to bias. For example, Let X be a random variable with cumulative distribution $F(x)$, and quantile function $x(F)$, a sample order statistics of a random sample size r, $X_{k:r}$, can be drawn from the distribution of X (Valbuena et al., 2017). Therefore, L-moments of X result from their expected values $E(X_{k:r})$ as expressed in Equations 1, 2, and 3 for the first, second, and third L-moments respectively (Hosking, 1990, Hosking, 1989).

$$L1 = EX = \int_0^1 x(F)dF \quad (1)$$

$$L2 = \frac{1}{2}E(X_{2:2} - X_{1:2}) = \int_0^1 x(F)(2F-1)dF \quad (2)$$

$$L3 = \frac{1}{3}E(X_{3:3} - 2X_{2:3} + X_{1:3}) = \int_0^1 x(F)(6F^2 - 6F + 1)dF \quad (3)$$

For forest plot decay level estimation, X represents the distribution of ALS heights of the trees in the plots. L-coefficient of variation (*Lcv*) and L-skewness (*Lskew*) are types of L-moment ratios such that (Adnan et al., 2021, Valbuena et al., 2017):

$$Lcv = \frac{L2}{L1} \quad (4)$$

And

$$Lskew = \frac{L3}{L2} \quad (5)$$

From Equations 4 and 5, Valbuena et al., (2017) proposed two rules (*Lcv* = 0.5 (Valbuena et al., 2012); and *Lskew* = 0) for discriminating tree sizes and assessing light availability in forest areas based on ALS height returns. Here, the rules are tested to discriminate and classify five forest plot decay levels into two categories from ALS height returns. We hypothesize that the ability of ALS pulses to reach subcanopies and provide a 3D structural view of canopies should show the variations in plot decay levels, due to variations in tree sizes and plot patterns. Consequently, while discriminating the variations in decay level, *Lcv* = 0.5 is tested to classify forest plot decay levels into two groups. *Lskew* = 0 is tested to classify forest plot decay levels into two groups, to detect areas where much light intensity can reach subcanopies; *Lskew* < 0 describes areas where more ALS light is backscattered due to closed canopies, while *Lskew* > 0 describes areas where light can easily reach subcanopies, due to forest gaps. Figure 3 illustrates the flowchart of the approach.

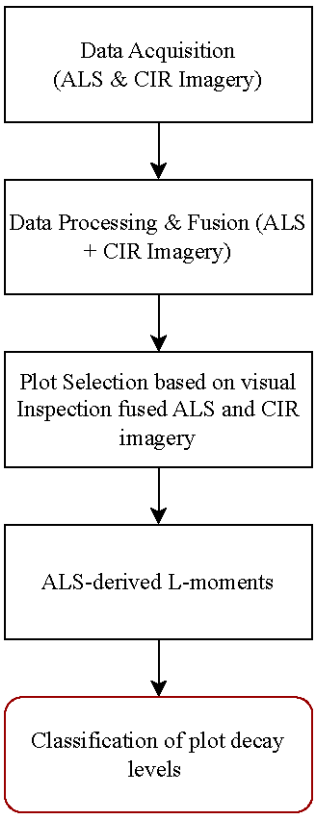

Figure 3. Flowchart of the approach

3. Results

Figure 4 displays the classification results of the plot decay levels based on the L-moments for the rule *Lcv = 0.5* from ALS height returns. From Equation 4, the rule in terms of L-moments can be expressed as $L2 = 0.5L1$, which represents the threshold that classifies the plot decay levels into two groups (areas of even sizes and areas of great inequality). Observation of the graph shows that the threshold (short blue dashes) categorized decay Levels 1 and 2 at *Lcv* < 0.5 and decay levels 3, 4, and 5 at *Lcv* > 0.5, although two plots from decay level 3 are lightly veered off the threshold. While the clusters of plots for each decay level are seen, the declining trend from Level 1 to Level 5 is observed. Moreover, the closeness of decay Levels 2 and 3 is worth noting.

Figure 5 shows the classification results of the plot decay levels based on L-moments for the rule *Lskew* = 0 from ALS height returns. The threshold (short blue dashes) represents the line of symmetry. Observation of the graph shows that decay Level 1 (healthy trees) is categorized at *Lskew* < 0, while decay levels 2 to 5 (dead trees) are categorized at *Lskew* > 0. It is also noteworthy the discrimination of clusters for each decay level, albeit the closeness of decay Levels 2 and 3.

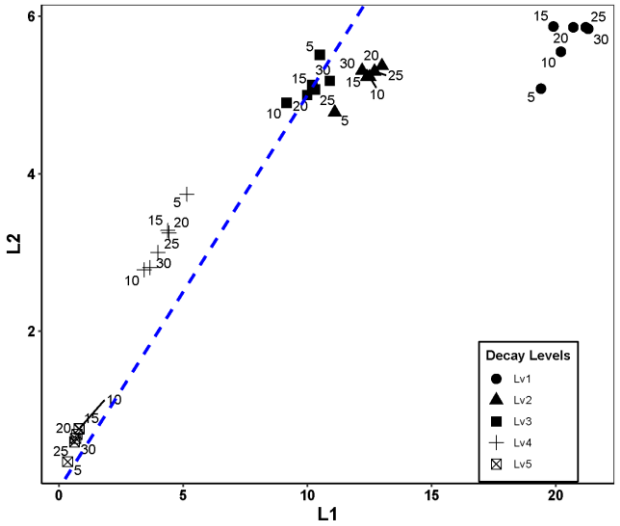

Figure 4. Classification of plot decay levels based on the rule *Lcv = 0.5* (short blue dashes). Numbers indicate respective plot radii.

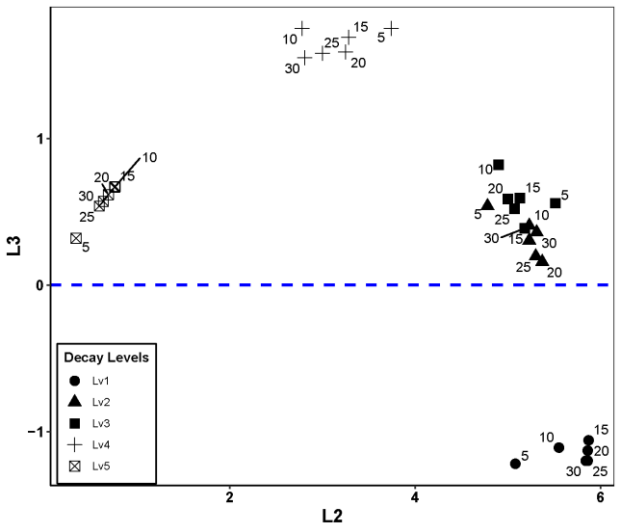

Figure 5. Classification of Classification of plot decay levels based on the rule *Lskew = 0* (short blue dashes). Numbers indicate respective plot radii.

4. Discussion

LiDAR-based ALS-derived L-moments can directly classify forest structural features (Adnan et al., 2021, Valbuena et al., 2017). Cognizant of the fact that the effect of tree decay results in biophysical changes in tree canopy structure and sizes, we hypothesized that ALS-derived L-moments can directly discriminate forest plot decay levels and serve as an optional convenient approach to understanding forest growth dynamics without field data. Thus, we tested the two proposed L-moment-based rules (Valbuena et al., 2017) to discriminate and classify forest plot decay levels into two categories from ALS height returns. Our results show that the first rule, *Lcv* = 0.5 (Figure 4) classified decay Levels 1 and 2 as even-sized areas (*Lcv* < 0.5), while decay Levels 3, 4, and 5 were classified as areas of great size inequality (*Lcv* > 0.5). This indicates that plot decay Levels 1 and 2 are forest areas where trees are even sized while Levels 3, 4, and 5 are areas of great

inequality. However, Level 2 despite being categorized as an even-sized area could be seen closer to the threshold boundary and to Level 3. While this indicate a small difference between decay Level 2 and 3, it further confirms that the Level 2 plot consists of early- stage dead trees, which may have a slight structural deficiency in decay (defoliation). This also demonstrates the reason why it is sometimes challenging to differentiate between Level 2 and 3, and 1 and 2 from only ALS point clouds; thus showing the necessity of the sensor combination in assessing decay levels (Wong et al., 2023). Moreover, the findings indicate that there exists a dependency between the first L-moment (L1) and the second L-moment (L2) as the declining trend of decay levels is demonstrated in Figure 4, which equally reflects the decline in tree heights from decay Level 1 to 5. This further implies that ALS-derived L-moments, especially the relationship between L1 and L2, have the potential for modeling forest plot decay levels.

On the other hand, results for the second rule, $Lskew = 0$ (Figure 5) classified decay Level 1 as closed canopy areas ($Lskew < 0$) while decay Levels 2 to 5 are classified as open canopy areas ($Lskew > 0$). This corroborates the concept of forest plot decay levels and their effects. For example, dense forests with healthy trees (Level 1) have closed canopies. However, when trees die and begin to decay, gaps begin to widen, and the degree of decay is proportional to the extent of gaps in the canopies and forests. Also, this explains that the second rule has the potential to classify forest areas of healthy trees and areas of dead trees. This further implies that the second rule categorized forest areas where ALS light pulses do not easily reach the understory due to closed canopy, resulting in backscattering at the higher canopy levels (like the concept of Euphotic zone (Lefsky et al., 2002b, Lefsky et al., 1999), and forest areas where the ALS light pulses can easily reach the understory due to canopy gaps and tree size inequalities (like the concept of oligophotic zones (Lefsky et al., 2002b, Lefsky et al., 1999). These findings exhibit the significance of LiDAR metrics in classifying forest plot decay levels for understanding forest growth dynamics. The approach can be simple and convenient to forest managers for understanding forest growth dynamics for effective forest management. Furthermore, while forest managers can exploit this approach for mapping areas of large gaps for planning and managing forest resources, the approach can equally be significant for assessing forest biomass, biodiversity, and carbon stock.

5. Conclusion

In this study, we directly discriminated and classified five forest plot decay levels from LiDAR-based ALS height returns using L-moments. The classification resulted from testing two proposed L-moment-based rules ($Lcv = 0.5$ and $Lskew = 0$). The first rule, $Lcv = 0.5$, classified plot decay levels based on tree structural sizes, and thus classified Levels 1 and 2 at $Lcv < 0.5$ indicating forest areas of even-sized trees, while Levels 3, 4, and 5 were classified at $Lcv > 0.5$ indicating forest areas of great size inequality. On the other hand, the second rule $Lskew = 0$ classified plot decay levels based on the amount of ALS light intensity, and thus classified Level 1 at $Lskew < 0$ indicating forest areas where most light intensity is backscattered due to closed canopy, while Levels 2 to 5 were classified at $Lskew > 0$ indicating forest areas where most light intensity reaches sub-canopy due to open canopy. The research provides an optional and convenient approach forest managers can use, in the absence of field data, to understand forest growth dynamics through the discrimination and classification of forest plot decay levels. Also, the approach can be exploited for mapping forest areas with large gaps for planning and managing forest resources effectively.

Acknowledgements

The authors would like to acknowledge the effort of all researchers involved and to thank the Department for National Park Monitoring and Animal Management of the Bavarian Forest National Park, Germany, for providing the data used in this study. This study was also supported by the National Natural Science Foundation of China (Project No. 42171361) and the Research Grants Council of the Hong Kong Special Administrative Region, China, under Project PolyU 25211819.

References

Adnan, S., Maltamo, M., Mehtätalo, L., Ammaturo, R. N., Packalen, P., Valbuena, R., 2021. Determining maximum entropy in 3D remote sensing height distributions and using it to improve aboveground biomass modelling via stratification. *Remote Sensing of Environment*, 260, 112464.

Curtis, P. G., Slay, C. M., Harris, N. L., Tyukavina, A., Hansen, M. C., 2018. Classifying drivers of global forest loss. *Science*, 361(6407), 1108–1111.

Dong, P., Chen, Q., 2017. LiDAR remote sensing applications CRC Press.

Drake, J. B., Dubayah, R. O., Knox, R. G., Clark, D. B., Blair, J. B., 2002. Sensitivity of large-footprint lidar to canopy structure and biomass in a neotropical rainforest. *Remote Sensing of Environment*, 81, 378-392.

Dubayah, R. O., Drake, J. B., 2000. Lidar remote sensing for forestry. *Journal of forestry*, 98(6), 44–46.

FAO, 2020. *Global forest resources assessment 2020: Main report*. Food & Agriculture Organization of the UN.

Gauthier, S., Bernier, P., Kuuluvainen, T., Shvidenko, A. Z., Schepaschenko, D. G., 2015. Boreal forest health and global change. *Science*, 349(6250), 819–822.

Hansen, M. C., Potapov, P. V., Moore, R., Hancher, M., Turubanova, S. A., Tyukavina, A., Thau, D., Stehman, S. V., Goetz, S. J., Loveland, T. R. et al., 2013. High-resolution global maps of 21st-century forest cover change. *Science*, 342(6160), 850-853.

Hosking, J. R. M., 1989. Some theoretical results concerning L-moments. *Research Report, RC 14492*, 1-9.

Hosking, J. R. M., 1990. L-Moments: Analysis and Estimation of Distributions Using Linear Combinations of Order Statistics. *Journal of the Royal Statistical Society: Series B (Methodological)*, 52, 105-124.

Keen, F. P., 1955. The Rate of Natural Falling of Beetle-Killed Ponderosa Pine Snags. *Journal of Forestry*, 53, 720-723. https://academic.oup.com/jof/article/53/10/720/4684777.

Lausch, A., Erasmi, S., King, D. J., Magdon, P., Heurich, M., 2016. Understanding forest health with remote sensing part I—a review of spectral traits, processes and remote-sensing characteristics. *Remote Sensing*, 8(12), 1029.

Lausch, A., Erasmi, S., King, D. J., Magdon, P., Heurich, M., 2017. Understanding forest health with remote sensing-part II—A review of approaches and data models. *Remote Sensing*, 9(2), 129.

Lefsky, M. A., Cohen, W. B., Acker, S. A., Parker, G. G., Spies, T. A., Harding, D., 1999. Lidar Remote Sensing of the Canopy Structure and Biophysical Properties of Douglas-Fir Western Hemlock Forests. *Remote Sensing of Environment*, 70, 339-361.

Lefsky, M. A., Cohen, W. B., Harding, D. J., Parker, G. G., Acker, S. A., Gower, S. T., 2002a. Lidar remote sensing of above-ground biomass in three biomes. *Global Ecology and Biogeography*, 11, 393-399.

Lefsky, M. A., Cohen, W. B., Parker, G. G., Harding, D. J., 2002b. Lidar Remote Sensing for Ecosystem Studies. *BioScience*, 52, 19-30.

Millar, C. I., Stephenson, N. L., 2015. Temperate forest health in an era of emerging megadisturbance. *Science*, 349(6250), 823–826.

Nielsen, M. M., Heurich, M., Malmberg, B., Brun, A., 2014. Automatic mapping of standing dead trees after an insect out-break using the window independent context segmentation method. *Journal of forestry*, 112(6), 564–571.

Roussel, J. R., Auty, D., Coops, N. C., Tompalski, P., Good-body, T. R., Meador, A. S., Bourdon, J. F., de Boissieu, F., Achim, A., 2020. lidR: An R package for analysis of Airborne Laser Scanning (ALS) data. *Remote Sensing of Environment*, 251, 112062.

Sani-Mohammed, A., Wong, T.-C., Yao, W., Heurich, M., 2023. Deep learning-based tree decay level classification from combined airborne lidar data and CIR imagery.

Sani-Mohammed, A., Yao, W., Heurich, M., 2022. Instance segmentation of standing dead trees in dense forest from aerial imagery using deep learning. *ISPRS Open Journal of Photogrammetry and Remote Sensing*, 6, 100024.

Sugden, A., Fahrenkamp-Uppenbrink, J., Malakoff, D., Vignieri, S., 2015. Forest health in a changing world.

Teobaldelli, M., Cona, F., Saulino, L., Migliozzi, A., D’Urso, G., Langella, G., Manna, P., Saracino, A., 2017. Detection of diversity and stand parameters in Mediterranean forests using leaf-off discrete return LiDAR data. *Remote Sensing of Environment*, 192, 126-138.

Thomas, J., 1979. *Wildlife habitats in managed forests: the Blue Mountains of Oregon and Washington*. 553, US Department of Agriculture.

Valbuena, R., Maltamo, M., Mehtätalo, L., Packalen, P., 2017. Key structural features of Boreal forests may be detected directly using L-moments from airborne lidar data. *Remote Sensing of Environment*, 194, 437-446.

Valbuena, R., Packalén, P., Martı, S., Maltamo, M. et al., 2012. Diversity and equitability ordering profiles applied to study forest structure. *Forest Ecology and Management*, 276, 185–195.

van der Knaap, W. O., van Leeuwen, J. F., Fahse, L., Szidat, S., Studer, T., Baumann, J., Heurich, M., Tinner, W., 2020. Vegetation and disturbance history of the Bavarian Forest National Park, Germany. *Vegetation History and Archaeobotany*, 29, 277-295. https://link.springer.com/article/10.1007/s00334-019-00742-5.

White, J. C., Coops, N. C., Wulder, M. A., Vastaranta, M., Hilker, T., Tompalski, P., 2016. Remote sensing technologies for enhancing forest inventories: A review. *Canadian Journal of Remote Sensing*, 42(5), 619–641.

Wingfield, M., Brockerhoff, E., Wingfield, B. D., Slippers, B., 2015. Planted forest health: the need for a global strategy. *Science*, 349(6250), 832–836.

Wong, T., Sani-Mohammed, A., Yao, W., Heurich, M., 2023. Automatic Classification of Single Tree Decay Stages from Combined ALS Data and Aerial Imagery using Machine Learning. *arxiv.org*. https://arxiv.org/abs/2301.01841.

Yao, W., Krzystek, P., Heurich, M., 2012. Tree species classification and estimation of stem volume and DBH based on single tree extraction by exploiting airborne full-waveform LiDAR data. *Remote Sensing of Environment*, 123, 368–380.

Zhang, W., Qi, J., Wan, P., Wang, H., Xie, D., Wang, X., Yan, G., 2016. An Easy-to-Use Airborne LiDAR Data Filtering Method Based on Cloth Simulation. *Remote Sensing 2016, Vol. 8, Page 501*, 8, 501.